J. Min. Metall. Sect. B-Metall. 59 (2) (2023) 205 - 216

Journal of Mining and Metallurgy, Section B: Metallurgy

STUDY ON THE DRYING CHARACTERISTICS OF GREEN PELLETS OF ULTRAFINE IRON ORE CONCENTRATE

B.-L. Wen [a], X.-P. Zhang [a,b], D.-L. Liu [c], J.-X. Li [a], X.-D Sun [a], J.-L. Yang [a,*]

[a] School of Metallurgical Engineering, Anhui University of Technology, Anhui, China;
[b] Ma'anshan Iron and Steel Co. Ltd., Anhui, China,
[c] Fushun New Steel Co. Ltd., Liaoning, China

(Received 10 August 2022; Accepted 04 June 2023)

Abstract

*Ultrafine iron ore concentrate pose challenges such as poor pellet formation performance, low-bursting temperature, and a complex drying thermal regime. To examine the drying characteristics of green pellets made from ultrafine iron ore concentrate, the Weibull distribution function and Dincer model were employed to fit and analyze the corresponding drying curve. The effects of drying temperature and air speed on the strength of dried pellets were also studied. The findings revealed that the drying process of green pellets of ultrafine iron ore concentrate involved three stages: ascending speed, constant speed, and descending speed. As the drying temperature and air speed increased, the drying time decreased. The coefficient of determination R^2 for the fitted Weibull distribution function model ranged from 0.995 to 0.998, while the R^2 value for the Dincer model ranged from 0.990 to 0.996. Both fitted models aligned with the experimental data and proved to be effective. According to the Bi values obtained through the Dincer model, raising the drying air speed in the initial stage and the drying air temperature in the subsequent stage of the drying system could efficiently remove moisture, reduce the risk of green pellet rupture, and maintain productivity. The moisture diffusion coefficient and convective mass transfer coefficient increased with rising temperature and air velocity, following the order of Deff > Dcal > D*eff as determined by the Weibull distribution function, Dincer model, and Fick's second law. Additionally, the activation energy value of ultrafine iron ore concentrate for drying derived from the Arrhenius formula was 4515.60 J/(mol·K). Notably, increasing the drying temperature increased the strength of the dried particles due to their more compact and dense internal structure. This study offers theoretical support for simulating the drying of green ultrafine iron ore concentrate pellets and provides guidelines for selecting diverse drying conditions and designing drying equipment.*

Keywords: *Ultrafine iron ore concentrate; Pellets; Weibull distribution function; Dincer model; Moisture diffusivity*

1. Introduction

Pelletized iron ore is a widely used high-quality iron-making material in blast furnace production due to its unique benefits, which include enhancing the utilization rate of the blast furnace, improvingcolumn permeability, reducing air pollutants, and facilitating transportation [1]. In the past decade, the steel industry has experienced significant growth, leading to an increase in the pellets ore feed ratio annually. As a result, mining operations have had to resort to deep fine grinding and magnetic separation processes to obtain iron ore concentrate with acceptable total iron (TFe) grades but ultrafine particle sizes [2,3]. However, ultrafine iron ore concentrate fines can have an adverse effect on the permeability and productivity of sinter beds [4–9], pellets processing is still the preferred option [10,11].Green pellets drying is a crucial intermediate stage between green pellets preparation and pellets preheating and roasting. In this process, convective heat transfer via hot air is utilized to facilitate moisture removal [12]. However, due to the high density of ultrafine iron ore concentrate green pellets, they have a low resistance to pellets bursting during drying, making the process more complex and demanding [13]. To avoid pellets bursting and ensure optimum moisture removal while reducing condensation within the material layer, strict temperature control is necessary [14,15]. Research on the green pellets drying process has largely focused on developing drying models that can predict moisture changes and aid in process optimization and regulation. For instance, Anna-Lena Ljung [16] employed computational fluid dynamics (CFD) to study the convective drying of individualiron ore pellets. Her research identified four stages involved in the drying process. Maycon Athayd [17] used microwave-assisted drying to demonstrate its

Corresponding author: jialongyang@126.com

https://doi.org/10.2298/JMMB220810018W

Table 1. *Chemical composition of ultrafine iron ore concentrate (mass%)*

Raw material	Chemical composition								L_{OI}
	TFe	FeO	CaO	SiO_2	MgO	Al_2O_3	P	S	
ultrafine iron ore concentrate powders	66.58	28.88	0.12	6.75	0.58	0.06	0.01	0.01	-2.2

effectiveness in enhancing the drying rate of iron ore pellets. The main drying models currently employed include the Lewis, Henderson-Pabi, Page, Wang-Singh, and shrinkage kernel models [18]. However, the parameters of these models, whichare derived from regression calculations of moisture ratio and drying time, often lack transparency, failing to accurately depict the heat and mass transfer phenomena involved in the drying process, particularly when different methods and processes are combined. Instead, models such as the Weibull distribution function and Dincer model/parameters offer more meaningful insights. These models have been applied successfully in fields such as materials science, pharmacology, and agronomy for analysis and optimization of drying processes for plants such as chrysanthemums [19] grapes [20], and papayas [21]. Despite the success of these models, their application in simulations of the drying process of ultrafine iron ore concentrate green pellets is yet to be seen. Therefore, this paper employs the Weibull distribution function and Dincer model to analyze the drying characteristics curve and heat and mass transfer mechanism of green pellets of ultrafine iron ore concentrate. The paper includes calculation of the drying activation energy and effective moisture diffusion coefficient of green pellets. Furthermore, it investigates the effects of drying temperature and air speed on the strength of the drying pellets to provide theoretical support for the prediction and regulation of the drying process of ultrafine iron ore concentrate pellets.

2. Experimental materials and methods

2.1. Experimental materials

A Chinese mining company supplied an ultrafine iron ore concentrate for testing. The source has over 1 billion tons of geological reserves, primarily aqueous poor ore with 30-40% Fe grade. The chemical composition and X-ray diffraction analysis of the ultrafine iron ore concentrate fines are presented in

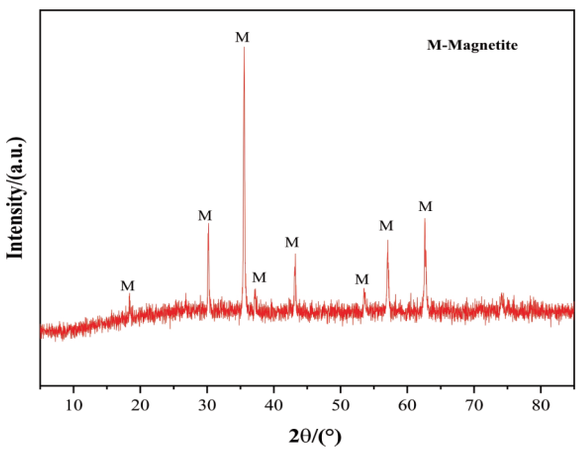

Figure 1. *X-ray diffraction analysis of ultrafine iron ore concentrate*

Table 1 and Fig. 1. The concentrate was high in Fe grade (>65%) and low in harmful impurities such as P and S, with magnetite being the main component. Table 2 and Fig. 2 describe the physical properties and microscopic morphology of the ultrafine iron ore concentrate, respectively. The ultrafine iron ore concentrate also had weak pellets Forming Properties (with a pellets Forming Properties index of 0.31). Scanning electron microscopy (JSM6490) revealed that the mineral powder particle surface had a smooth, mostly plate-like structure, making it difficult for microfine particles to adhere and participate in the spherification process [22] . Table 3 and Table 4 list the physical and chemical properties of the bentonite.

2.2. Experimental Methods

The experimental disc pelletizer featured a diameter of 1000 mm, a disc height of 200 mm, a rotational speed of 23 r/min, and a disc inclination of 47°.To meet laboratory and pellets plant pellets diameter requirements and minimize the impact of pellets diameter on drying speed and quality, only

Table 2. *Ultrafine iron ore concentrate physical properties (mass%)*

Raw material	>0.074 mm	0.048–0.074mm	0.038–0.048mm	0.025–0.038mm	<0.025 mm	S_{BET}/ ($m^2 \cdot g^{-1}$)	Sphericity index
ultrafine iron ore concentrate	0	1.46	3.65	10.33	84.56	0.604	0.31

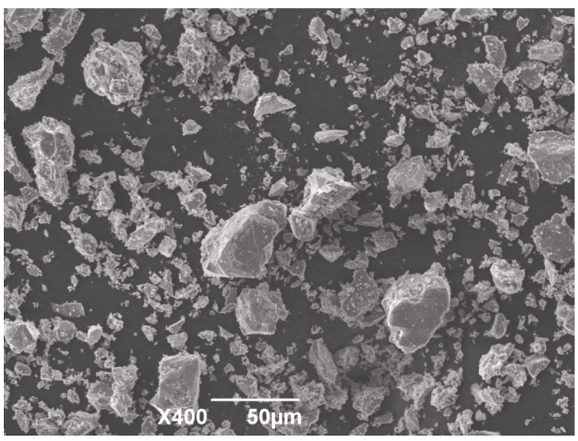

Figure 2. *Micromorphology of ultrafine iron ore concentrate*

Table 3. *Chemical constituents of bentonite (mass%)*

Chemical composition								L_{OI}
TFe	FeO	CaO	SiO_2	MgO	Al_2O_3	P	S	
5.13	0.21	2.96	56.74	2.14	14.96	0.051	0.046	11.73

Table 4. *Chemical composition of ultrafine iron ore concentrate (mass%)*

Methylene blue absorption/ (g $(100g)^{-1}$)	Montmorillonite mass fraction/%	Colloidal valence/ ($ml \cdot g^{-1}$)	Swelling capacity/ ($ml \cdot g^{-1}$)	2h water absorption/%
29.6	74.4	355	11	341.1

pellets with diameters between 12 and 13 mm were utilized in studying drying characteristics. This choice also reduced the effect of pellets size on the drying process, ultimately reinforcing the dependability and precision of experimental outcomes.

Pellets were immediately dried after preparation using the apparatus depicted in Fig. 3. For every drying test, 50 green pellets were dried at different temperatures (100, 150, 200, 250, and 300°C) and drying air velocities (1.0, 1.2, 1.4, 1.6, and 1.8 m/s). The mass was recorded every 30 seconds during drying, and three repeat tests were conducted in parallel. The final values were determined by averaging the data.

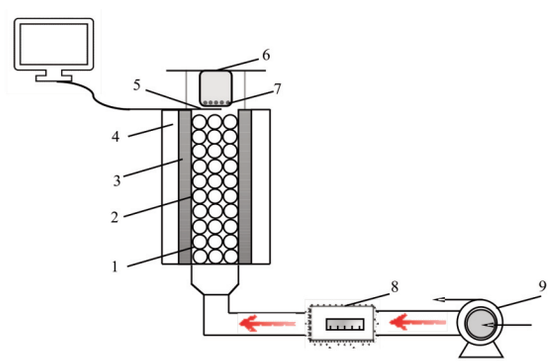

1-Alumina balls、2-Hot air duct、3-Heating strip、4-Heat Insulation Strip、5-Thermocouple、6-Drying Cup、7- 50 green pellets、8-Flowmeter、9-Blower

Figure 3. *Diagram of drying test equipment*

The compressive strength of the dried pellets was determined using a particle strength tester (YHKC-2A). Twenty pellets were tested each time and the peak strength of each pellet was recorded. After excluding the maximum and minimum values, the average value of the remaining data was taken as the result, expressed in N/pellet.

The microstructure of the dried pellets was observed using a scanning electron microscope (JSM6490).

2.3. Drying curve fitting and parameter calculation method

2.3.1. Drying parameters calculation

The moisture ratio (M_R) was used to express the water content of the raw ultrafine concentrate pellets during the drying process. The moisture ratio at different times t is shown in equation (1) [18]

$$M_R = \frac{M_t}{M_0} \tag{1}$$

where M_t, M_0 denotes the water content of the green pellets at any t moment and the initial dry basis during drying, respectively, corresponding to how many g of water per gram of dry basis,the unit of M_R is g/g.

The drying rate (DR) is calculated using equation (2).

$$D_R = \frac{M_{t1} - M_{t2}}{t_2 - t_1} \tag{2}$$

where M_{t1} and M_{t2} denote the dry based on the moisture content of the pellets at times t_1 and t_2 during drying, respectively, the unit of D_R is g/(g·s).

2.3.2. Weibull distribution function

Originally used to describe material stresses, the Weibull model has also been successfully applied in recent years to describe chemical and microbial

degradation processes, as well as the kinetics of changes in drying processes. The Weibull distribution function is shown in equation (3).

$$M_R = \exp\left[-\left(\frac{t}{\alpha}\right)^{\beta}\right] \quad (3)$$

Where α is the proportionality parameter, which can be considered as a reaction kinetic constant equal to the time when the drying process is 63% complete, and β is the shape parameter, which is related to the initial mass transfer rate and moisture migration mechanism.

The estimation of moisture diffusion coefficient of the drying process (D_{cal}) can be estimated using the Weibull distribution function, and the equation is equation (4).

$$D_{cal} = \frac{r^2}{\alpha} \quad (4)$$

where D_{cal} is the estimated moisture diffusion coefficient in m^2/s; r is the equivalent-volume radius of the material, i.e., the radius of the raw sphere, taking the average value of 0.00625 m.

2.3.3. Dincer Model

Dincer proposed the Dincer model based on the similarity of temperature variation and drying characteristic curves, as shown in equation (5) [23].The Dincer model can analyze the drying process and help to solve the diffusion coefficient and heat and mass transfer coefficient.

$$M_R = G\exp(-St) \quad (5)$$

where G is the model hysteresis factor, which can reflect the internal resistance to heat transfer and heat transfer process of green pellets drying; S is the drying coefficient, which can show the drying capacity of the material in unit time; and t is the corresponding-drying time, s.

According to Dincer and Hussain, for spherical materials, the Biovor number (Bi) and moisture diffusivity (D_{eff}) can be derived from the model hysteresis factor G and drying coefficient S, as shown in equations (6) and (7).

$$Bi = 0.0576G^{26.7} \quad (6)$$

$$D_{eff} = \frac{S \cdot r^2}{\mu^2} \quad (7)$$

In equation (7), r is the characteristic dimension (radius of the sphere), here is the radius of the raw sphere, and the r value is taken as 0.00625 m; μ is the root of the characteristic equation (8) [24].

$$\mu = -8.3256G^4 + 54.84G^3 - 134.01G^2 + 145.83G - 58.124 \quad (8)$$

From equations (6), (7), and (8) combined with equation (9), the convective mass transfer coefficient k is obtained.

$$k = \frac{D_{eff} Bi}{r} \quad (9)$$

2.3.4. Calculation of effective diffusion coefficient of water

A simplified Fick's law was used to describe the moisture migration law in the drying phase of spherical materials, as shown in equation (10) [25].

$$\ln(M_R) = \ln\left(\frac{6}{\pi^2}\right) - \pi^2 \frac{D^*_{eff} t}{r^2} \quad (10)$$

where D^*_{eff} is the effective moisture diffusion coefficient, m/s; r is the radius of the raw sphere 0.00625 m; t is the drying time, s. Equation (10) by plotting the experimental drying data of $\ln M_R$ with time, the D^*_{eff} value can be calculated, and the slope can be obtained by linear regression of $\ln M_R$ with the time curve, and then the effective moisture diffusion coefficient can be derived from the slope of the straight line.

2.3.5. Activation energy calculation

The result of activation energy of drying can reflect the degree of difficulty of drying materials and estimate the energy consumption of drying. The activation energy of dried green pellets was calculated using the Arrhenius formula, as shown in equation (11).

$$\ln D^*_{eff} = \ln D_0 - \frac{E_a}{R(T + 273.15)} \quad (11)$$

where D_0 is the frequency factor (constant) m^2/s; E_a is the activation energy, J/mol; R is the molar gas constant, 8.314 J/(mol·K); T is the material drying temperature, ℃. The formula (11) $\ln D^*_{eff}$ and T are linearly fitted to obtain the drying activation energy E_a.

2.3.6. Data processing and analysis

The cardinality test was used in this study to test whether the distributions of continuous variables such as drying time and moisture ratio were consistent with the results of the two model fits involved in the above paper. Origin 8.5 software was used for regression

analysis of the experimental data, and the goodness of fit was evaluated by the coefficient of determination (R^2) equation (12) and the chi-square (χ^2) equation (13), where the higher the R^2 was the closer to 1 and the lower the χ^2 value, the better the fitting accuracy.

$$R^2 = 1 - \frac{\sum_{i=1}^{N}\left(M_{R\,pre,i} - M_{R\,exp,i}\right)^2}{\sum_{i=1}^{N}\left(\overline{M_{R\,pre,i}} - M_{R\,exp,i}\right)^2} \quad (12)$$

$$\chi^2 = \frac{\sum_{i=1}^{N}\left(M_{R\,exp,i} - M_{R\,pre,i}\right)^2}{N - z} \quad (13)$$

where $M_{Rexp,\,i}$ is the i·th moisture ratio measured in the experiment; $M_{Rpre,\,i}$ is the i·th moisture ratio predicted by the model used, all are dimensionless numbers, $\overline{M_{Rpre,\,i}}$ is the mean value of the moisture ratio predicted by the model; N is the number of data recorded in the experiment and z is the number of model constant terms.

3. Results and Analysis

3.1. Drying characteristics of pellets

The drying temperature is the most important influencing factor for drying the green pellets of ultrafine iron ore concentrate. If the temperature is too low, the moisture in the green pellets cannot evaporate in time and the production efficiency will be reduced; if the temperature is too high, the heat transfer process will be carried out rapidly due to the existence of the temperature gradient and the vapor pressure inside the pellets will increase, which will prompt the bursting of green pellets and reduce the permeability of the material layer and bring bad effects on the subsequent pellets oxidation roasting consolidation. Fig. 4 presents the variation of M_R and D_R with respect to time (t) in the drying characteristics curve of green pellets at five different drying temperatures, while maintaining a drying air speed of 1.4 m/s.

The water content inside the green ultrafine concentrate pellets gradually decreased with the extension of drying time in the M_R-t curve, and the required drying times were 570, 420, 330, 240, and 210 s at drying temperatures of 100, 150, 200, 250, and 300°C, respectively. The higher the temperature, the more favorable was the production efficiency.

The drying rate D_R-t curve could be divided into three stages: accelerating, constant, and decelerating. Increasing the temperature had a negligible impact on reducing the duration of the accelerating stage of drying. The rise in temperature intensified the evaporation of moisture, leading to a substantial boost in the drying rate. This effect helped shorten the timespan of both constant and decelerating stages of drying for green particles, as found similarly by Zhang Han-quan [18] in their experiments with artificial magnetite.

The impact of hot air drying speed on drying of green pellets was significant. Fig. 5 displays the M_R-t and D_R-t curves at various hot air drying speeds with a drying temperature of 200°C. The findings revealed that elevating the hot air drying speed could expedite drying time; at an increased hot air speed ranging from 1.0 to 1.8 m/s, the drying time decreased from 390 s to 240 s. Furthermore, increasing the hot air drying speed was conducive to enhancing the drying rate, owing to higher airflow speed reducing the vapor pressure on the surface of the green pellets and promoting the rapid diffusion of water vapor from its surface into the air.

3.2. Analysis of pellets drying curve fitting results

The results of fitting the drying characteristics curves of green pellets using the Weibull distribution function model at different drying temperatures and

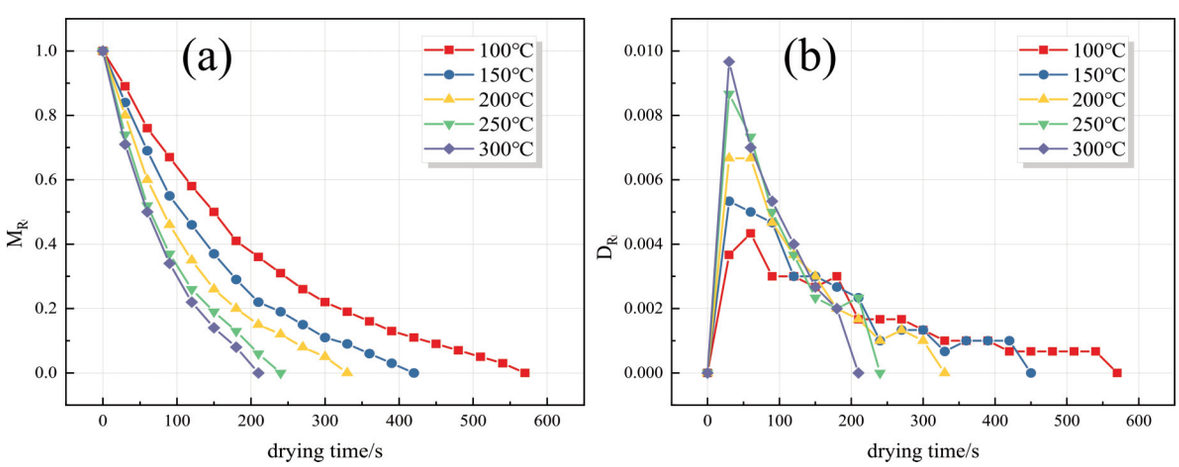

Figure 4. *Drying characteristic curve of green pellets of ultrafine iron ore concentrate at different temperatures (drying airspeed 1.4 m/s) (a) M_R-t curve (b) D_R-t curve*

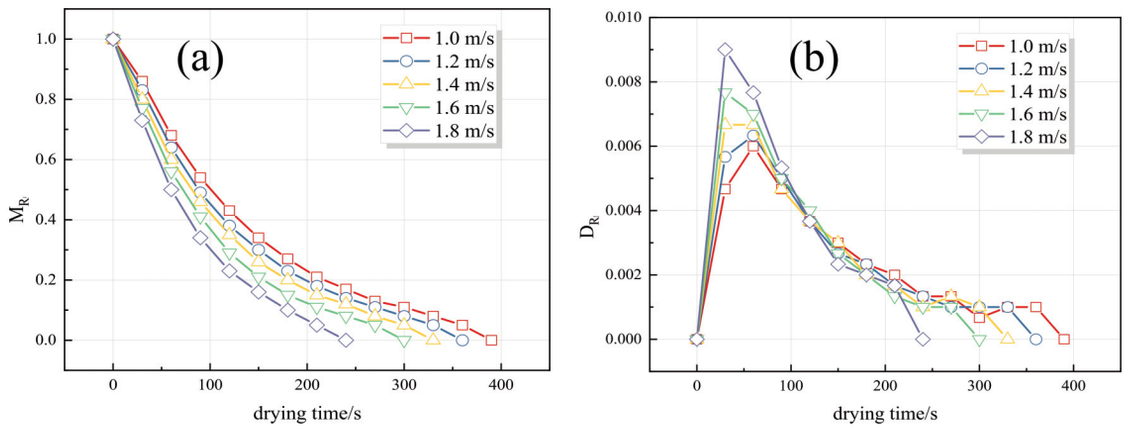

Figure 5. *Drying characteristic curve of green pellets of ultrafine iron ore concentrate at different air velocities (drying temperature 200°C) (a) M_R-t curve (b) D_R-t curve*

air velocities are shown in Table 5 and Fig. 6.

The α value was approximately the time required to complete 63% of the green pellets drying process from Table 5. In this, as the drying temperature increased from 100 °C to 300 °C the corresponding α_T value decreased from 204.415 s to 81.476 s, a 60.14% reduction in time. As the drying airspeed increased from 1.0 m/s to 1.8 m/s, the corresponding α_V value decreased from 141.179 s to 83.992 s, and the time was reduced by 40.51%, indicating that both increased the drying temperature and drying air speed could effectively reduce the drying time of the green pellets.

The shape parameter β was associated with water migration mechanisms during the drying process and material drying characteristics. When β was between 0.3 and 1, it suggested that the drying rate was considerably influenced by internal moisture diffusion control. Conversely, when β exceeded 1, the joint diffusion of internal and external moisture controlled the drying process. Table 5 shows, the value of β for ultrafine iron ore concentrate green pellets was in the range of 1.097 to 1.126, indicating that the drying rate was jointly controlled by internal and external moisture diffusion. The coefficient of determination (R^2) rangesd from 0.995 to 0.998, and the cardinality (χ^2) ranged between 1.505×10^{-4} and 5.567×10^{-4}. Moreover, the Weibull distribution function provided a better fit for the drying curve.

The results of fitting the curve of green pellets drying characteristics based on the Dincer model at different drying temperatures and air velocities are shown in Table 6 and Fig. 7.

Table 6 displays The G_T and G_v values that ranged from 1.019 to 1.034 and 1.022 to 1.038, respectively, which exceeded 1 and suggested an increase in drying rate during the initial stage. Additionally, the drying coefficient S, an indicator of drying ability, progressively increased as S_T rose from 5.150×10^{-3} to 12.810×10^{-3} and S_V increased from 7.490×10^{-3} to 12.430×10^{-3}, illustrating the effectiveness of higher temperatures and air volumes in improving the drying capacity of green particles. The Dincer model provided a satisfactory fit for the curve, as evidenced

Table 5. *Results of fitting the drying characteristics curve of green pellets of ultrafine iron ore concentrate based on the Weibull distribution function model*

Drying temperature/°C	Weibull distribution model fitting results (dry air speed 1.4 m·s^{-1})			
	α_T/s	β_T	R_T^2	χ_T^2
100	204.415	1.126	0.998	1.741×10^{-4}
150	147.286	1.124	0.998	2.091×10^{-4}
200	114.258	1.097	0.998	2.214×10^{-4}
250	89.804	1.12	0.995	5.143×10^{-4}
300	81.476	1.157	0.995	5.567×10^{-4}
Drying air speed/(m·s^{-1})	Weibull distribution model fitting results (drying temperature 200°C)			
	α_V /s	β_V	R_V^2	χ_V^2
1	141.179	1.14	0.998	2.221×10^{-4}
1.2	125.952	1.11	0.998	2.281×10^{-4}
1.4	114.258	1.097	0.998	2.214×10^{-4}
1.6	99.641	1.108	0.998	1.505×10^{-4}
1.8	83.992	1.137	0.998	2.600×10^{-4}

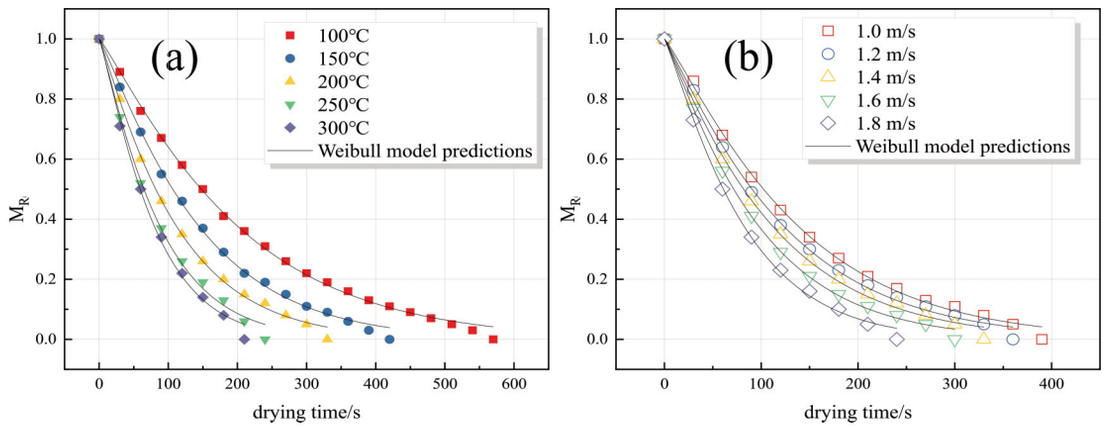

Figure 6. *Comparison of predicted and true values of the Weibull distribution function model;* ***(a)*** *Comparison between the predicted and real values of the drying characteristics curve of green pellets of ultrafine iron ore concentrate at different temperatures (drying air speed 1.4 m/s) based on the Weibull distribution function model;* ***(b)*** *Comparison between the predicted and real values of the drying characteristics curve of green pellets of ultrafine iron ore concentrate at different air speeds (drying temperature 200°C) based on the Weibull distribution function model*

by R^2 transitioning from 0.990 to 0.996 and χ^2 ranging from 11.700×10^{-4} to 3.884×10^{-4}.

The model parameters, effective water diffusion coefficient, and activation energy calculation results obtained from the Weibull model and Dincer model are shown in Table 7 and Table 8.

The Bi value is a measure that reflects the ratio of internal thermal conductivity and surface convective heat transfer resistance of dry media and materials, as expressed in equation (14), where:, δ represents the characteristic length, h represents the surface heat transfer coefficient, and λ Represents the thermal conductivity of a solid.

$$\mathrm{Bi} = \frac{\delta \mathrm{h}}{\lambda} \tag{14}$$

Bi values ranging from 0 to 0.1 were indicative of convective heat transfer resistance at the surface primarily governing the temperature fluctuations of the sample, whereas values between 0.1 and 100 suggested the combined role of internal heat transfer resistance and surface convective heat transfer resistance in regulating temperature variations during the drying process. When the drying temperature exceeded 200 °C, with drying airflow velocities at 1.4 m/s and Bi values less than 0.1, increasing temperature could reduce the drying time of green spheres. However, exceeding a certain temperature threshold may lead to uneven temperature distribution inside the green spheres. While increasing air speed had a limited effect on Bi values, raising the blast drying speed could decrease the moisture content of green spheres, leading to decreased burst temperature and reduced drying time.

Therefore, it was suggested that the drying system could increase the drying wind speed in the early stage and the drying wind temperature in the later

Table 6. *Results of fitting the drying characteristics curve of green pellets of ultrafine iron ore concentrate based on the Dincer model*

Drying temperature/°C	Dincer model fitting results (dry air speed 1.4 m·s^{-1})			
	G_T	S_T /s^{-1}	R_T^2	χ_T^2
100	1.034	5.150×10^{-3}	0.995	4.528×10^{-4}
150	1.029	7.120×10^{-3}	0.995	5.111×10^{-4}
200	1.022	9.080×10^{-3}	0.996	4.111×10^{-4}
250	1.019	11.550×10^{-3}	0.992	8.623×10^{-4}
300	1.02	12.810×10^{-3}	0.99	11.700×10^{-4}
Drying air speed/(m·s^{-1})	Dincer model fitting results (drying temperature 200°C)			
	G_V	S_V /s^{-1}	R_V^2	χ_V^2
1	1.038	7.490×10^{-3}	0.994	5.475×10^{-4}
1.2	1.029	8.300×10^{-3}	0.996	4.399×10^{-4}
1.4	1.022	9.080×10^{-3}	0.996	4.111×10^{-4}
1.6	1.022	10.430×10^{-3}	0.996	3.884×10^{-4}
1.8	1.022	12.430×10^{-3}	0.994	6.898×10^{-4}

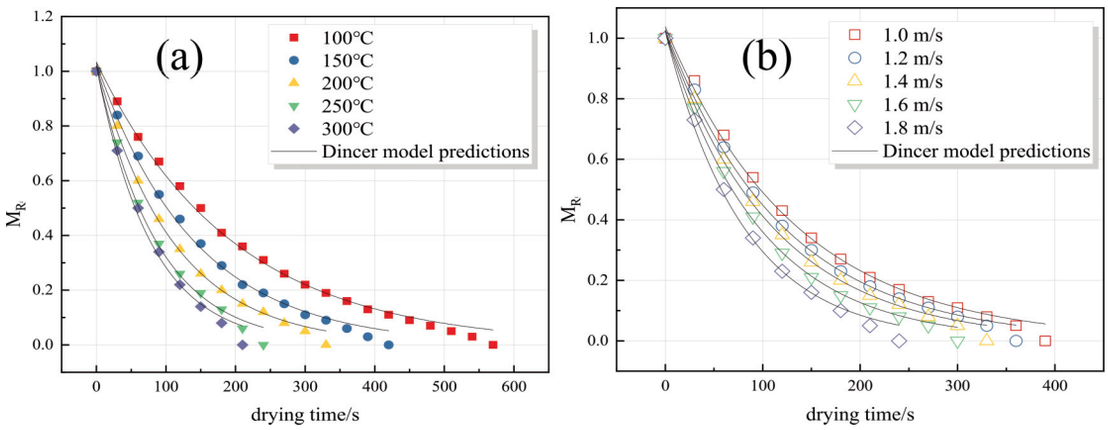

Figure 7. *Comparison of predicted and true values of the Dincer model under different drying conditions;* ***(a)*** *Comparison between the predicted and real values of the drying characteristics curve of green pellets of ultrafine iron ore concentrate (drying air speed 1.4 m/s) at different temperatures based on the Dincer model;* ***(b)*** *Comparison between the predicted and real values of the drying characteristics curve of green pellets of ultrafine iron ore concentrate (drying temperature 200°C) at different air speeds based on the distribution function model of the Dincer model*

stage to ensure effective removal of moisture, reduce the risk of green pellets breakage, and maintain productivity. The predicted moisture changes using Weibull and Dincer models could also optimize the regulation of the drying process.

The increase in drying temperature and wind speed was beneficial for improving the water mass transfer coefficient k. From 100 °C to 300 °C, the mass transfer coefficient increased by 189.09%. As the drying wind speed increased from 1.0 m/s to 1.8 m/s, the mass transfer coefficient increased by 90.09%.

The moisture diffusion coefficients obtained based on the Weibull model, Dincer model, and Fick's second law all increased with increasing temperature. The moisture diffusion coefficient $D_{eff}>D_{cal}>D^*_{eff}$ mainly considered: (1) The prerequisite for the calculation of D^*_{eff} was that the entire drying process was always in the deceleration drying stage, ignoring the acceleration stage caused by heat transfer in the early stage of drying and the constant velocity stage achieved by the transient diffusion of water vapor from the inside of the green pellets through the capillary formed by iron ore particles to the surface of the green pellets, the estimated value was low; (2) The Weibull model and Dincer model were based on the actual water diffusion characteristics of the material, and the high Deff may be mainly due to their calculation measuring the influence of internal thermal resistance and external thermal resistance and mass transfer coefficient of the material.

The drying activation energy (E_a) value was related to the substances that combine with water in the green pellets and the internal structure of the green

Table 7. *Calculated results of parameters obtained from Weibull model and Dincer model at different drying temperatures*

Drying temperature/°C	$D_{calT}/m^2\cdot s^{-1}$	$D_{effT}/m^2\cdot s^{-1}$	$D^*_{effT}/m^2\cdot s^{-1}$	Bi_T	$k_T/m\cdot s^{-1}$
100	1.911×10^{-7}	0.819×10^{-6}	3.166×10^{-8}	0.141	1.842×10^{-5}
150	2.652×10^{-7}	1.335×10^{-6}	3.483×10^{-8}	0.124	2.640×10^{-5}
200	3.419×10^{-7}	2.219×10^{-6}	3.799×10^{-8}	0.103	3.656×10^{-5}
250	4.350×10^{-7}	3.207×10^{-6}	4.354×10^{-8}	0.095	4.886×10^{-5}
300	4.794×10^{-7}	3.405×10^{-6}	5.462×10^{-8}	0.098	5.325×10^{-5}

Table 8. *Calculated results of parameters obtained from the Weibull and Dincer models at different drying wind speeds*

Drying air speed/$(m\cdot s^{-1})$	$D_{calv}/m^2\cdot s^{-1}$	$D_{effV}/m^2\cdot s^{-1}$	$D^*_{effV}/m^2\cdot s^{-1}$	Bi_V	$k_V/m\cdot s^{-1}$
1	2.767×10^{-7}	1.055×10^{-6}	2.335×10^{-8}	0.156	2.633×10^{-5}
1.2	3.104×10^{-7}	1.557×10^{-6}	3.245×10^{-8}	0.123	3.078×10^{-5}
1.4	3.419×10^{-7}	2.219×10^{-6}	3.799×10^{-8}	0.103	3.656×10^{-5}
1.6	3.920×10^{-7}	2.549×10^{-6}	4.987×10^{-8}	0.103	4.199×10^{-5}
1.8	4.651×10^{-7}	3.037×10^{-6}	5.501×10^{-8}	0.103	5.005×10^{-5}

pellets. In this study, according to the Arrhenius formula, the activation value of green pellets drying was 4515.60 J/(mol·K).

3.3. Drying pellets strength

Pellets drying strength is a vital indicator of pellets drying quality. Fig. 8 illustrates the impact of drying temperature and drying air velocity on the strength of dried ultrafine iron ore concentrate pellets. At various drying temperatures, the strength of dried pellets exceeded 22 N/pellets [26,27] and increased by approximately 10 N/pellets with rising temperature. Conversely, the effect of drying air velocity on the drying temperature was insignificant. As demonstrated in Fig. 9 elevating the temperature boosted the strength of ultrafine concentrate pellets by enhancing the internal vapor pressure of the pellets, which facilitated the dispersion of iron ore fines and resulted in more compact dried pellets.

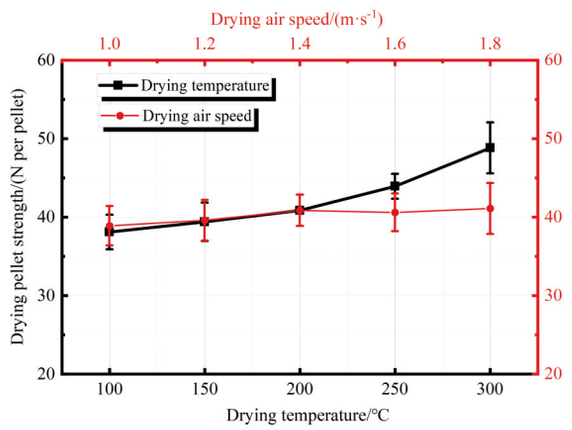

Figure 8. *Drying pellets strength at different drying temperatures and drying air speeds*

4. Conclusions

1. The drying process of green pellets made from ultrafine iron ore concentrates comprised three stages: acceleration, constant, and deceleration. Increasing the drying temperature and the drying air speed could reduce the drying time effectively. The R2 value for the coefficient of determination of the Weibull distribution function model for the drying characteristics curve of green pellets ranged from 0.995 to 0.998, and that of the Dincer model ranged from 0.990 to 0.996. The fitted results of both models matched the experimental data, proving their effectiveness.

2. Elevating the drying temperature and airspeed could shorten the drying time and enhance drying capacity of green pellets. Both internal and external moisture diffusion played a role in determining the drying rate. The Bi values obtained through the Dincer model proposed that raising the drying air speed in the initial stage and the drying air temperature in the subsequent stage of the drying system could facilitate efficient moisture elimination, diminish rupture risk of green pellets, and maintain productivity.

3. The moisture diffusion coefficient and convective mass transfer coefficient rose with an increase in temperature and air velocity, according to

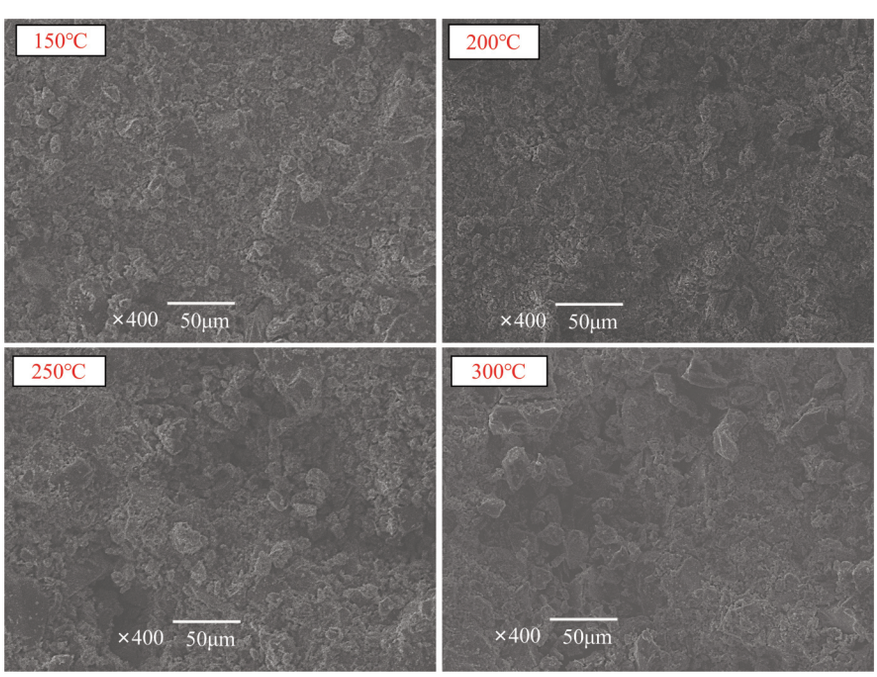

Figure 9. *Micromorphology of drying pellets sections at different drying temperatures*

the Weibull distribution function, Dincer model, and Fick's second law. The values follow the order of Deff > Dcal > D*eff, the drying activation energy value of ultrafine iron ore concentrate derived from the Arrhenius formula was 4515.60 J/(mol·K).

4. The increase in drying temperature led to an increase in the strength of the dried particles of ultrafine iron ore concentrate due to their more compact and dense internal structure at higher temperatures. This study provided theoretical support for simulating the drying of green ultrafine iron ore concentrate pellets and provided a reference for selecting various drying conditions and designing drying equipment.

Acknowledgements

The authors would like to thank A grant from the National Natural Science Foundation of China (NO.U1860113) for providing funding to complete the experiments

Author's contributions

B.-L. Wen conducted experiments and data analysis, and wrote a manuscript. X.-P. Zhang and X.-D. Sun participated in the experiment and provided constructive suggestions for the article. D.-L. Liu, along with J.-X. Li and J.-L. Yang, participated in the experiment and provided financial support.

Conflict of interest statement

We declare that all authors have no conflict of interest.

Data Availability Statement

The processed data needed to reproduce these findings cannot be shared at this time, as they also form part of an ongoing study, in accordance with the funder's data retention policy.

References

[1] M. Xu, W. Wang, J. Sun, X.S. Zhang, Application on low carbon smelting technology for feeding large percentage of pellets into super-large BF, China Metallurgy, 31 (2021) 98-103 (in Chinese). https://doi.org/10.13228/j.boyuan.issn1006-9356.20210349

[2] G. F. Gao, X. L. Zhou, Z. ShiandL. P. Liu. 2021. Study on the kinetics of gas-solid based synergistic reduction of limonite carbon-containing pellets, Journal of Mining and Metallurgy, Section B: Metallurgy, 57(2) 185-193. https://doi.org/10.2298/JMMB200510017G.

[3] D. Zhu, J. Pan, L. Lu, R.J. Holmes, Iron ore, Woodhead Publishing, Cambridge, UK, P.435.

[4] F.Q. Gu, Y.B. Zhang, G.H. Li, Q. Zhong, J. Luo, Z.J. Su, M.J. Rao, Z.W. Peng, T. Jiang, Effective preparation of blast furnace burdens from superfine iron concentrates by composite agglomeration process, Ironmaking & Steelmaking, 47 (2020) 908-914. https://doi.org/10.1080/03019233.2019.1641681

[5] J. T. Ju, C.M. Tang, Z.G. Pang, X.D. Xingand, G.H. Ji, Effect of high MgO/Al_2O_3 ratio (1.2 to 2.2) on sintering behavior and metallurgical properties, Journal of Mining and Metallurgy, Section B: Metallurgy, 57(1) (2021) 21-30. https://doi.org/10.2298/JMMB200330034J.

[6] S.Z. He, H.L. Feng, M. Gan, X.J. Gan, Effects of characters of ultra fine iron ore concentrate on sinter, Journal of Iron and Steel Research, 27 (2015) 6-12 (in Chinese). https://doi.org/10.13228/j.boyuan.issn1001-0963.20140058

[7] D.Q. Zhu, M.J.Xu, J. Pan, C.C. Yang, H.Y. Tian, Experimental research to improve pelletsability of ultrafine concentrate, Journal of Iron and Steel Research, 29 (2017) 704-710 (in Chinese). https://doi.org/10.13228/j.boyuan.issn1001-0963.20160387

[8] M.S. Zhou, Y.D. Wang, D.M Zhao, H.L. Han, X.C. Li, L.M. Lu, Development on sintering technologies with high proportion of magnetite concentrates, Iron and Steel, 55 (2020) 1-9 (in Chinese). https://doi.org/10.13228/j.boyuan.issn0449-749x.20190304

[9] F. Zhang, D.Q. Zhu, J. Pan, Z.Q Guo, M.J. Xu. J, Characteristics of Western Australia Ultrafine (WAU) magnetite concentrates and their influence on pellets roasting performance, Journal of Iron and Steel Research International, 27 (2020) 770-781 (in Chinese). https://doi.org/10.13403/j.sjqt.2016.06.074

[10] J. Pal, S. Ghorai, T. Venugopalan, Effect of high Blaine iron ore fines in hematite ore pelletization for blast furnace, Mineral Processing and Extractive Metallurgy, 129 (2020) 299-307. https://doi.org/10.1080/25726641.2018.1505208

[11] Y.F. Li, T. Yang, Z.C. Liu, J.H. Zhou, J. Lei, P. Wang, Effect of high pressure roller grinding on the green pellets properties of ultrafine iron concentrate containing pyrite cinder, Journal of Iron and Steel Research, 34 (2022) 639-647 (in Chinese). https://doi.org/10.13228/j.boyuan.issn1001-0963.20210220

[12] J.Y. Fu, T. Jiang, D.Q. Zhu, Principle of sintering and pelletizing, Central South University of Technology Press, Changsha, China, P.205.

[13] G. Wong, X.H. Fan, M. Gan, Z.Y Ji, X.L Chen, Z.Y Tian, Z.Z Wang, Improvement on the thermal cracking performance of pellets prepared from ultrafine iron ore concentrate, Powder Technology, 342 (2019) 873-879. https://doi.org/10.1016/j.powtec.2018.08.090

[14] A.L. Ljung, T.S. Lundström, B.D. Marjavaara, K Tano, Influence of air humidity on drying of individual iron ore pellets, Drying Technology, 29 (2011) 1101-1111. https://doi.org/10.1080/07373937.2011.571355

[15] X.H. Fan, Z.Y. Tian, M. GAN, X.U. Chen, X.W. Zhou, G.J. Wang, Optimization of pore structure of fine-grained magnetite concentrate pellets, Mining and Metallurgical Engineering, 38 (2018) 71-75 (in Chinese). https://doi.org/10.3969/j.issn.0253-6099.2018.01.016

[16] A.L. Ljung, T.S Lundström, B.D. Marjavaara, K, Tano,

Convective drying of an individual iron ore pellets – Analysis with CFD, International Journal of Heat and Mass Transfer, 54 (2011) 3882-3890. https://doi.org/10.1016/j.ijheatmasstransfer.2011.04.040

[17] M. Athayde, M. Cota, M. Covcevich, Iron ore pellets drying assisted by microwave: A kinetic evaluation, Mineral Processing and Extractive Metallurgy Review, 39 (2018) 266-275. https://doi.org/10.1080/08827508.2017.1423295

[18] H.Q. Zhang, C.X Liu, M.M. Lu, H. Yu, Kinetic model research on drying characteristics of artificial magnetite green pellets, Journal of Central South University, 28 (2021) 89-99. https://doi.org/10.1007/s11771-021-4588-y

[19] X.F Cheng, Ling. Pan, N. Li, J.Q, Chen, Moisture diffusivity characteristics and model fitting of Jerusalem artichoke (Helianthus tuberosus L.) during microwave vacuum drying, Science and Technology of Food Industry, 43 (2022) 33-40 (in Chinese). https://doi.org/10.13386/j.issn1002-0306.2021070048

[20] J.W. Bai, J.L. Wang, H.W. Xiao, H.Y. Ju, Y.H.Liu Z.J Gao, Weibull distribution for modeling drying of grapes and its application, Transactions of the Chinese Society of Agricultural Engineering, 29 (2013) 278-285 (in Chinese). https://doi.org/10.3969/j.issn.1002-6819.2013.16.035

[21] H.Y. Ju, H.Y. Zhao, J. Zhang, W.P Zhang, X.L. Yu, J.Q. Wang, Z.J. Gao, H.W. Xiao, Drying characteristics of Chaenomeles sinensis with different drying methods based on Dincer model, Chinese Traditional and Herbal Drugs, 51 (2020) 3911-3921 (in Chinese). https://doi.org/10.7501/j.issn.0253-2670.2020.15.010

[22] A. Abazarpoor, M. Halali, Investigation on the particle size and shape of iron ore pellets feed using pellets mill and HPGR grinding methods, Physicochemical Problems of Mineral Processing, 53 (2017) 9080-919. http://dx.doi.org/10.5277/ppmp170219

[23] I. Dincer, M. M. Hussain, Development of a new Biot number and lag factor correlation for drying applications, International Journal of Heat and Mass Transfer, 47 (2004) 653-658. https://doi.org/10.1016/j.ijheatmasstransfer.2003.08.006

[24] W.A.M. McMinn, Prediction of moisture transfer parameters for microwave drying of lactose powder using Bi–G drying correlation, Food Research International, 37 (2004) 1041-1047. https://doi.org/10.1016/j.foodres.2004.06.013

[25] U. Sahin, H.K. Öztürk, Effects of pulsed vacuum osmotic dehydration (PVOD) on drying kinetics of figs (Ficus carica L), Innovative Food Science and Emerging Technologies, 36 (2016) 104-111. https://doi.org/10.1016/j.ifset.2016.06.003

[26] S.K. Kawatra, V.C. Laremboux, Iron ore pelletization: Part i. Fundamentals, Mineral Processing and Extractive Metallurgy Review, (2021) 1-20. https://doi.org/10.1080/08827508.2021.1947269

[27] B.L. Wen, X.P. Zhang, D.L Liu, J.X. Li, H.L Wu, J.L Yang, Effect of boron-containing magnetite on properties of ultrafine-grained magnetite pellets, Iron and Steel, 57 (2022) 33-41 (in Chinese). https://doi.org/10.13228/j.boyuan.issn0449-749x.20220357

ISTRAŽIVANJE O KARAKTERISTIKAMA SUŠENJA ZELENIH PELETA ULTRAFINOG KONCENTRATA GVOŽĐA

B.-L. Wen [a], X.-P. Zhang [a,b], D.-L. Liu [c], J.-X. Li [a], X.-D Sun [a], J.-L. Yang [a,*]

[a] Fakultet metalurškog inženjerstva, Univerzitet za tehnologiju Anhui, Anhui, Kina
[b] Ma'anshan Iron and Steel Co. Ltd, Anhui, Kina
[c] Fushun New Steel Co. Ltd, Liaoning, Kina

Apstrakt

*Ultrafini koncentrat gvožđa predstavlja izazove kao što su loša performansa formiranja peleta, niska temperatura pucanja i složeni termalni režim sušenja. Da bi se ispitale karakteristike sušenja sirovih peleta ultrafinog koncentrata gvožđa, primenjene su Weibulova distribuciona funkcija i Dincerov model kako bi se prilagodili i analizirali odgovarajuće krive sušenja. Takođe su proučeni efekti temperature sušenja i brzine vazduha na čvrstoću osušenih peleta. Rezultati su pokazali da sušenje sirovih peleta ultrafinog koncentrata gvožđa prolazi kroz tri faze: faza rasta brzine, konstantna brzina i faza opadanja brzine. Kako su temperatura sušenja i brzina vazduha rasle, vreme sušenja se smanjivalo. Koeficijent determinacije R^2 za prilagođeni model Weibulove distribucione funkcije kretao se od 0,995 do 0,998, dok je vrednost R^2 za Dincerov model bila u opsegu od 0,990 do 0,996. Oba prilagođena modela se poklapaju sa eksperimentalnim podacima i pokazala su se efikasnim. Prema vrednostima Bi dobijenim putem Dincerovog modela, povećanje brzine sušenja vazduha u početnoj fazi i temperature sušenja vazduha u kasnijoj fazi sušenja mogu efikasno ukloniti vlagu, smanjiti rizik od pucanja zelenih peleta i održavati produktivnost. Koeficijent difuzije vlage i koeficijent konvektivnog prenosa mase su se povećavali sa porastom temperature i brzine vazduha, prateći redosled Deff > Dcal > D*eff, kako je utvrđeno Weibulovom distribucionom funkcijom, Dincerovim modelom i Fikovim drugim zakonom. Takođe, aktivaciona energija ultrafinog koncentrata gvožđa za sušenje, izvedena iz Arrheniusove formule, iznosi 4515,60 J/(mol•K). Važno je napomenuti da povećanje temperature sušenja povećava čvrstoću osušenih čestica zbog njihove kompaktnije i guste unutrašnje strukture. Ovo istraživanje pruža teorijsku podršku za simuliranje sušenja zelenih peleta ultrafinog koncentrata gvožđa i pruža smernice za izbor različitih uslova sušenja i dizajniranje opreme za sušenje.*

Ključne reči: *Ultrafini koncentrat gvožđa; Peleti; Weibulova distribuciona funkcija; Dincerov model; Difuzivnost vlage*